Astron. Astrophys. 333, 1025–1033 (1998)

ASTRONOMY AND ASTROPHYSICS

Profile of CH_4 IR bands in ice mixtures

G. Mulas[1,2], **G.A. Baratta**[3], **M.E. Palumbo**[3], **and G. Strazzulla**[3]

[1] Dipartimento di Scienze Fisiche dell'Università di Cagliari, Via Ospedale 72, I-09124 Cagliari, Italy
[2] Osservatorio Astronomico di Cagliari, Str. 54, Loc. Poggio dei Pini, I-09012 Capoterra (CA), Italy
[3] Osservatorio Astrofisico di Catania, V.le A. Doria 6, I-95125, Catania, Italy

Received 11 November 1997 / Accepted 28 January 1998

Abstract. We studied the infrared spectral characteristics of frozen methane (CH_4) in several astrophysically relevant ice mixtures, as deposited and after ion irradiation. We examined the profile (shape, width and peak position) of the CH_4 bands as a function of initial mixture, irradiation dose and warming up temperature, and compared our results with previously published laboratory and observational data. Finally, we present a list of spectra that may be used for direct comparison with present and future observations.

Key words: molecular data – molecular processes – dust, extinction – ISM: molecules – infrared: ISM: lines and bands – methods: laboratory

1. Introduction

The presence of a considerable amount of CH_4 in dense molecular clouds has been predicted by a number of theoretical interstellar medium chemistry models, both of gas phase (e.g. Millar & Nejad, 1985; Herbst & Leung, 1986) and solid phase (e.g. Tielens & Hagen, 1982). Due to its high degree of symmetry, this molecule does not have a permanent dipole moment, and thus has no observable radio spectrum. On the other hand, it has two infrared active vibrational fundamentals (see e. g. Herzberg, 1991), the ν_4 C-H deformation mode at 1306 cm^{-1} (7.66 μm) and the ν_3 C-H stretching mode at 3020 cm^{-1} (3.31 μm), both measured in the gas phase. Due to the high atmospheric opacity at these wavelengths, only the feature at 7.66 μm has been looked for in ground based or air borne observations of bright protostars, and at rather low resolution and signal to noise ratio (Lacy et al., 1991; Boogert et al., 1997). These observations, while showing the presence of the CH_4 feature, did not permit to understand whether it was produced in the gas phase or in solid icy dust grain mantles. Recent ISO observations of the same feature (Boogert et al., 1996) set very low upper limits on the gas phase column density. Moreover, the profile of the absorption features suggests that most CH_4 should be embedded in polar icy grain mantles (H_2O or CH_3OH).

Laboratory experiments have shown that several effects are induced on ice mixtures after ion irradiation. In fact species are eroded from the target (sputtering, e.g. Johnson, 1990), the structure of the ice is modified (e.g. Baratta et al., 1991; Moore & Hudson, 1992), new molecular species both less volatile and more complex, not present in the initial samples, are formed (e.g. Moore et al., 1983; Strazzulla et al., 1997), along with a complex organic residue which is left over upon warmup (Strazzulla & Baratta, 1992). Here we present laboratory measures on the variation in shape and position of the two CH_4 features both in icy mixtures containing methane, as a function of composition of the ice, temperature and ion irradiation, and as produced after ion irradiation of mixtures containing CH_3OH. Since the shape and position of the peaks depend only weakly on the grain geometry, for ice mixtures containing less than 30% of CH_4 (see Boogert et al., 1997, for a discussion), many of our spectra can be compared directly to present and future observations, allowing some insight to be gathered on the chemical environment and irradiation history of the grain mantles in which CH_4 is embedded.

Send offprint requests to: G. Strazzulla

2. Experimental setup

A detailed description of the experimental apparatus used can be found elsewhere (Spinella et al., 1991). A stainless steel vacuum chamber, in which pressure is kept lower than 10^{-7} mbar, is faced through KBr windows to an FTIR spectrometer (4400 to 400 cm^{-1} = 2.27 to 25 μm). Inside the chamber, a silicon crystal substrate is placed in thermal contact with a cold finger that can be cooled down to 10 K. The gas or gas mixture to be investigated is injected into the chamber through a needle valve and immediately freezes on the substrate. All the spectra in this work have been ratioed to a background spectrum that includes the silicon wafer and were taken at a resolution of 2 cm^{-1}, and a sampling of 1 cm^{-1}. The samples can be bombarded during or after condensation by ions of energies ranging from 1.5 to 60 keV. Bombarding the samples during condensation makes it possible to prepare rather thick (several μm), uniformly irradiated films, while samples thinner than the penetration depth of the ions can be bombarded after deposition, enabling us to study the effects of irradiation at increasing doses. The ions are obtained from an ion gun (3 kV) or an ion implanter (30 kV). From this latter also doubly ionized Ar beams (60 keV Ar^{2+} ions) can be obtained. We used current densities ranging from

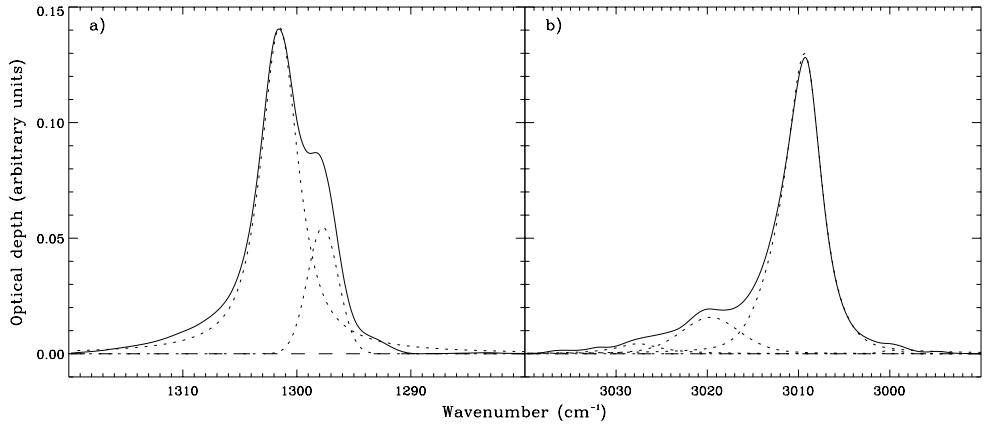

Fig. 1. a The profile of the band at 1302 cm^{-1} in pure CH_4 at T = 12.5 K (full line) and its resolution in two components (dotted lines). The band has been normalized to unit integrated area. **b** The profile of the band at 3010 cm^{-1} in pure CH_4 at T = 12.5 K (full line) and its resolution in components (dotted lines). The main peak is reproduced by the superposition of the second and third functions listed in Table 3. The band has been normalized to unit integrated area.

several 10^{-1} to not more than a few $\mu A \cdot cm^{-2}$ to avoid macroscopic heating of the target. The substrate plane forms an angle of about 45° with the ion beam and the IR beam. In this way, spectra can be taken at any time, before, during and after irradiation, with no need to tilt the sample. The energy released to the sample by impinging ions (dose) is given in eV per small molecule (16 a. m. u.) because this is a convenient scale to characterize the evolution of the samples upon irradiation and to compare results obtained irradiating different samples.

In some of the experiments, an He-Ne laser beam was used to monitor the thickness of the sample, by watching in real time the interference pattern between the reflections on the interfaces vacuum-sample and sample-substrate. In some experiments, moreover, the spectra were taken in polarized light, allowing us to minimize the effect of the variation of the real part of the refractive index across the band. In particular, the transmittance for light polarized perpendicularly to the plane of incidence depends strongly on the real part of the refractive index. This, for strong absorption can lead to the appearance of spurious features not due to absorption. By choosing a polarization in the plane of incidence, it is possible to eliminate almost completely this effect.

3. Results

The mid-infrared spectrum of solid methane shows four active bands, two fundamentals at 1302 cm^{-1} (7.68 μm, C-H ν_4 deformation mode) and 3010 cm^{-1} (3.32 μm, C-H ν_3 stretching mode), and two combination modes, the ν_1+ν_4 at 4203 cm^{-1} (2.38 μm) and the ν_3+ν_4 at 4303 cm^{-1} (2.32 μm). In this section we present a detailed study of the two fundamental modes in pure methane and ice mixtures, as deposited and after ion irradiation. All the spectra were first divided, in intensity scale, by a fitted continuum. Then they were converted to an optical depth scale, and peak positions and FWHM were taken. The intensity between sampled points were interpolated by cubic splines. The 1σ error in the peak position and the FWHM are estimated, from the noise level in the continuum, to be typically about 0.5 cm^{-1}, anyway always less than the sampling (1 cm^{-1}).

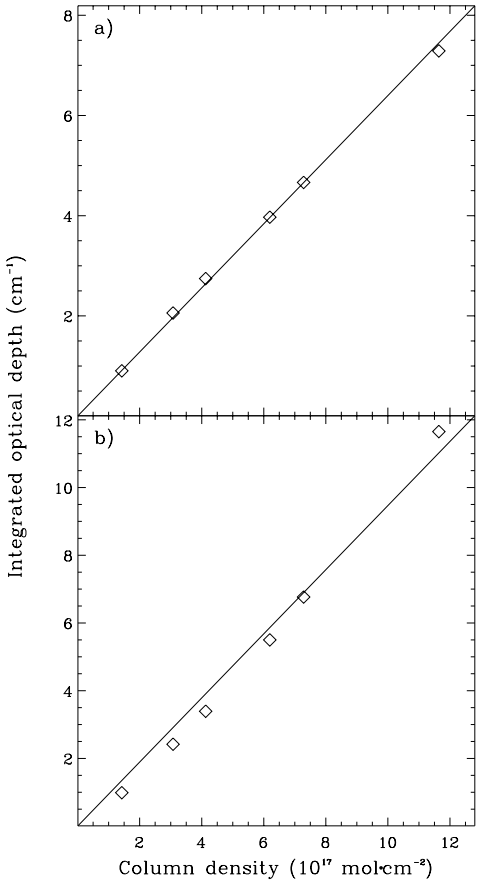

Fig. 2a and b. The points represent individual measures of the integrated optical depth of the CH_4 fundamental bands at 1302 cm^{-1} (inset **a**) and 3010 cm^{-1} (inset **b**) versus the column density of the sample, as deposited at T = 12.5 K. Superimposed is the line through the origin that best fits the points.

3.1. The 1302 cm^{-1} C-H deformation mode

Fig. 1a shows the profile of the ν_4 mode for pure CH_4 at T = 12.5 K, in optical depth scale and normalized to unit integrated area, at the end of the deposition.

It can be resolved in two components, that have been fitted with pseudo-voigt functions. A pseudo-voigt function is simply

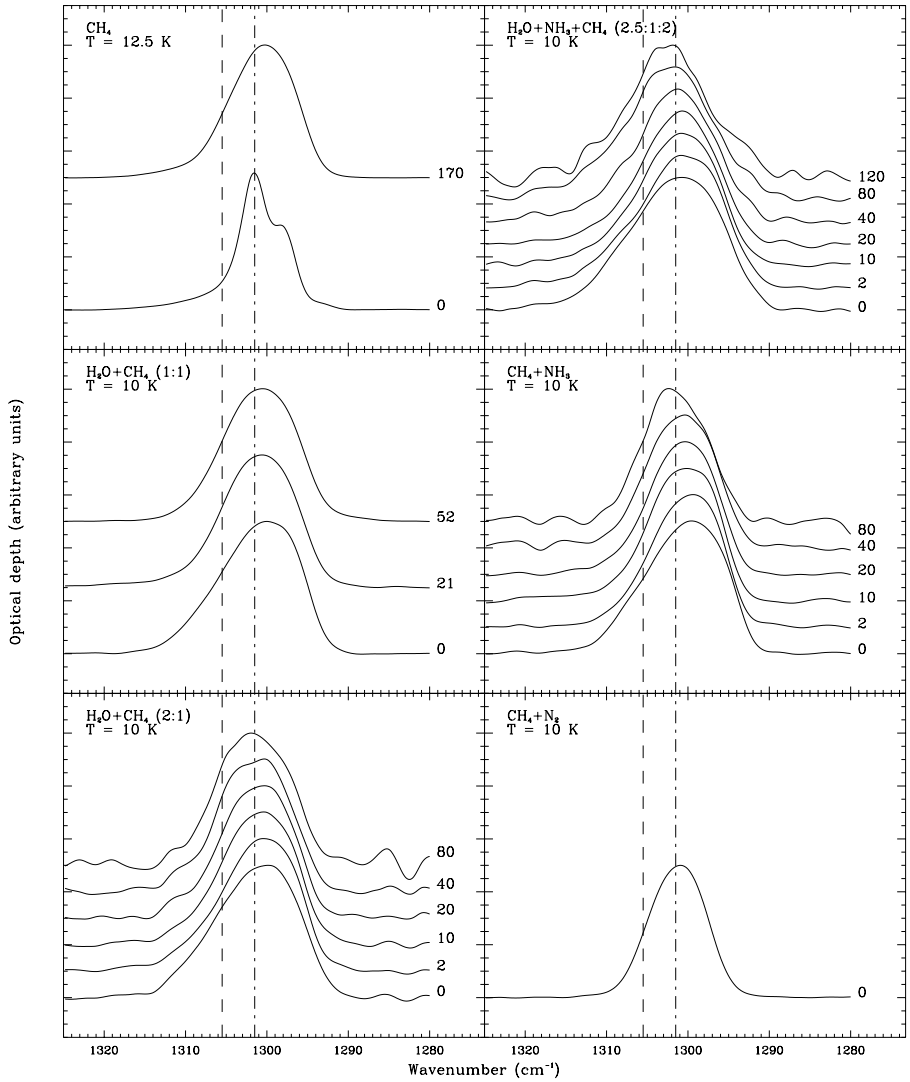

Fig. 3. Variations of the shape and position of the band at 1302 cm^{-1} of CH_4 codeposited in various ice mixtures upon increasing ion irradiation doses.The initial ice mixture is indicated in top left corner of each box, along with the temperature of the sample. The dose, in units of eV/16 a. m. u., is indicated beside each plotted band. The position of the origin of the band in gaseous CH_4 (1305.5 cm^{-1}) is indicated by the dashed line, the position of the peak in pure solid CH_4 as deposited (1301.5 cm^{-1}) is indicated by the dash-dotted line.

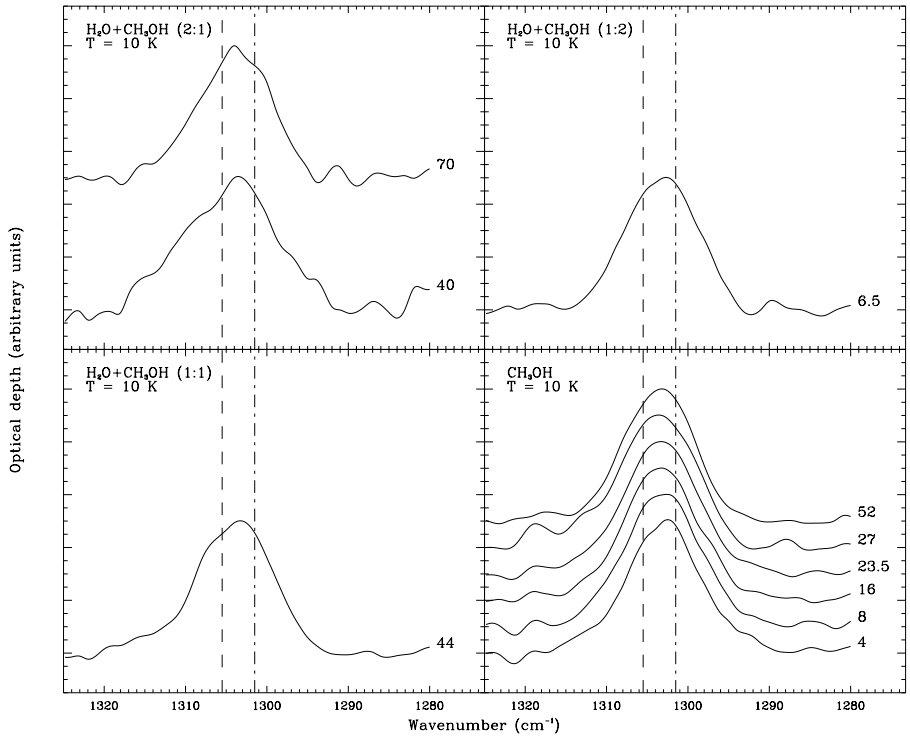

Fig. 4. Variations of the shape and position of the band at 1302 cm^{-1} of CH_4 produced by ion irradiation in various ice mixtures upon increasing doses.The initial ice mixture is indicated in top left corner of each box, along with the temperature of the sample. The dose, in units of eV/16 a. m. u., is indicated beside each plotted band. The position of the origin of the band in gaseous CH_4 (1305.5 cm^{-1}) is indicated by the dashed line, the position of the peak in pure solid CH_4 as deposited (1301.5 cm^{-1}) is indicated by the dash-dotted line.

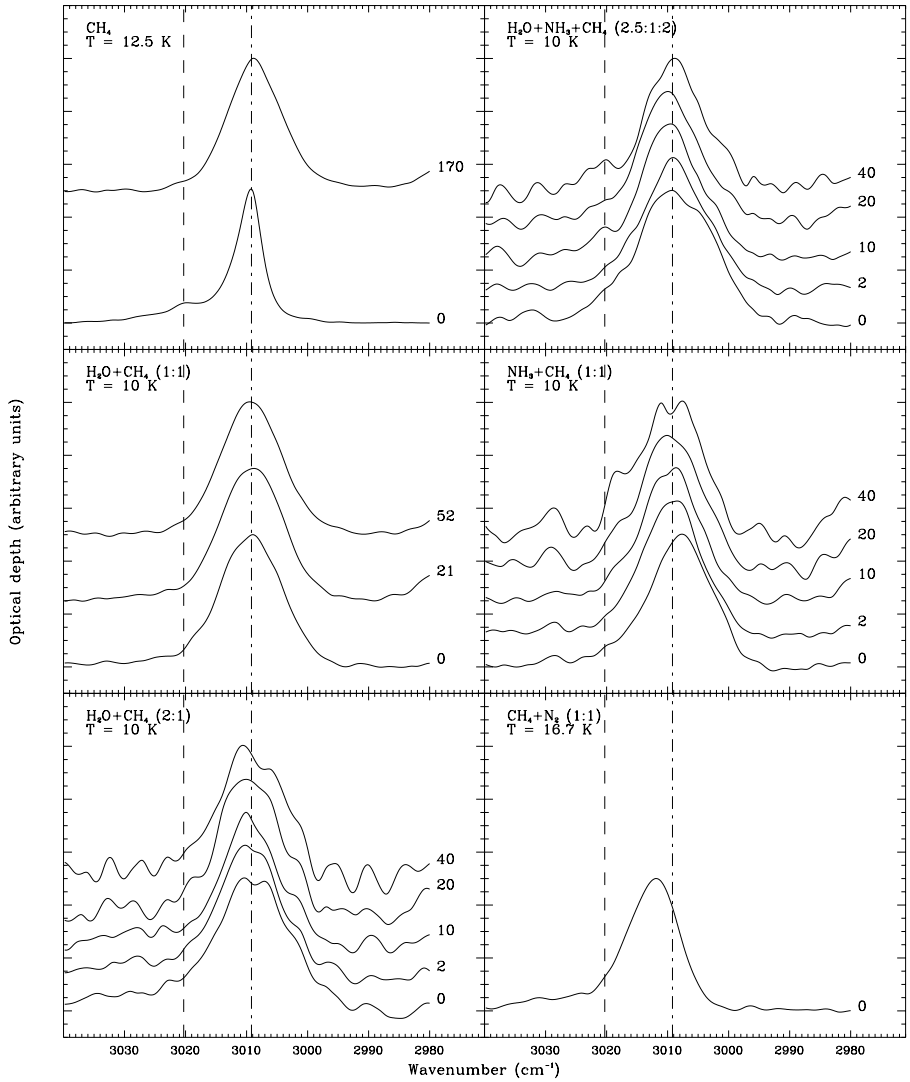

Fig. 5. The profiles of the band at 3010 cm^{-1} of CH_4 codeposited in various irradiated and unirradiated ice mixtures. The position of the origin of the band in gaseous CH_4 (3020.3 cm^{-1}) is indicated by the dashed line, the position of the peak in pure CH_4 ice as deposited (3009.2 cm^{-1}) is indicated by the dash-dotted line.

Table 1. The parameters of the pseudo-voigt functions that best fit the profile of the 1302 cm^{-1} band in pure CH_4 as deposited at T = 12.5 K.

Peak position cm^{-1}	FWHM cm^{-1}	η	Band area % of total
1297.7	3.2	0.00	18.5
1301.5	3.9	0.87	81.5

the weighted mean of a gaussian and a lorentzian with the same peak position and FWHM. A third parameter, η, gives the weight of the gaussian, and, consequently, $1 - \eta$ gives the weight of the lorentzian. The parameters were derived from a combined fit of all the spectra taken at various thicknesses of the sample, during its deposition. The parameters of the two fitting functions are shown in Table 1. The choice of the fitting functions has been just one of convenience to better reproduce the profile. The fitted profiles are shown dotted in Fig. 1a. While the fit is rather good, the main component in the experimental spectrum is slightly asymmetric, suggesting that the real profile may be more complex, possibly with more unresolved components.

The thickness of the pure CH_4 sample was measured during deposition from the interference fringes of a He-Ne laser beam reflected by the interfaces film-vacuum and film-substrate. Since the substrate is tilted of $45°$ with respect to the IR beam, the thickness traversed by the latter is approximately $\sqrt{2}$ times the measured thickness of the sample. We could therefore calculate the column density of CH_4 molecules in the path of the IR beam, using a density of solid CH_4 of 0.52 g cm^{-3} (Landolt-Börnstein 1971). Fig. 2a shows the points corresponding to the integrated optical depth of the band at various stages of the deposition, and thus various thicknesses, of the sample, plotted against the column densities of CH_4. The slope of the straight line through the origin fitted to the data yields a value of $6.4 \cdot 10^{-18}$ cm · mol^{-1} for the integrated absorbance. This value is somewhat smaller than that of $7.3 \cdot 10^{-18}$ cm · mol^{-1} derived by Boogert et al. (1997) based on data previously published by Hudgins et al. (1993).

The value of the integrated absorbance can not, at present, be measured when CH_4 is codeposited with other species, because we are not able to obtain an accurate estimate of the relative

Table 2. Position (cm^{-1}) and FWHM (cm^{-1}) of the 1302 cm^{-1} band of CH_4 in various ice mixtures at different doses of ion irradiation, all at low T (10-16 K). The dose is expressed in eV/16 a.m.u

Initial mixture	Ions used	Dose	Peak (cm^{-1})	FWHM (cm^{-1})
pure CH_4	He^+ 30 keV	0	1301.5	6.7
		170	1300.3	9.7
H_2O+CH_4 (1:1)	He^+ 3 keV	0	1300.6	12.0
		21	1300.8	10.8
		52	1300.5	11.0
H_2O+CH_4 (2:1)	He^+ 30 keV	0	1300.0	12.3
		2	1300.3	11.2
		10	1300.5	11.0
		20	1300.5	10.8
		40	1300.5	10.7
		80	1302.0	11.0
H_2O+NH_3+CH_4 (2.5:1:2)	He^+ 30 keV	0	1300.8	13.8
		2	1300.8	12.4
		10	1300.8	11.6
		20	1300.8	11.0
		40	1301.2	11.2
		80	1301.6	12.5
		120	1302.4	10.9
NH_3+CH_4 (1:1)	He^+ 30 keV	0	1299.4	12.0
		2	1299.3	10.4
		10	1300.0	10.3
		20	1300.3	9.9
		40	1300.4	10.2
		80	1302.1	9.6
N_2+CH_4 (1:1)	–	0	1301.0	8.4
H_2O+CH_3OH (2:1)	He^+ 3 keV	40	1303.4	12.8
		70	1304.0	10.4
H_2O+CH_3OH (1:1)	He^+ 3 keV	44	1303.3	10.9
H_2O+CH_3OH (1:2)	He^+ 3 keV	6.5	1303.6	10.9
CH_3OH	H^+ 30 keV	4	1302.5	10.3
		8	1302.8	11.1
		16	1303.2	10.7
		23.5	1303.2	10.7
	He^+ 3 keV	27	1303.6	11.2
		52	1303.2	10.3

Table 3. The parameters of the pseudo-voigt functions that best fit the profile of the 3010 cm^{-1} band in pure CH_4 as deposited at T = 12.5 K.

Peak position cm^{-1}	FWHM cm^{-1}	η	Band area % of total
2999.8	2.6	0.02	0.4
3009.0	3.3	0.45	27.3
3010.4	6.9	0.29	53.9
3019.6	7.6	0.34	14.4
3027.6	5.9	1.00	4.0

Table 4. Position (cm^{-1}) and FWHM (cm^{-1}) of the 3010 cm^{-1} band of CH_4 in various ice mixtures at different doses of ion irradiation, all at low T (10-16 K). The dose is expressed in eV/16 a.m.u

Initial mixture	Ions used	Dose	Peak (cm^{-1})	FWHM (cm^{-1})
pure CH_4	He^+ 30 keV	0	3009.2	5.2
		170	3008.9	10.4
H_2O+CH_4 (1:1)	He^+ 3 keV	0	3010.0	11.9
		21	3008.8	12.3
		52	3009.4	11.8
H_2O+CH_4 (2:1)	He^+ 30 keV	0	3008.7	14.6
		2	3009.4	12.0
		10	3010.0	10.1
		20	3009.9	11.5
		40	3010.0	12.8
		80	3010.0	10.0
H_2O+NH_3+CH_4 (2.5:1:2)	He^+ 30 keV	0	3008.9	14.7
		2	3009.0	12.2
		10	3009.5	11.0
		20	3010.0	11.4
		40	3008.9	10.7
		80	3009.0	13.0
		120	3009.4	12.0
NH_3+CH_4 (1:1)	He^+ 30 keV	0	3007.7	12.0
		2	3008.5	11.4
		10	3009.0	11.2
		20	3010.0	11.6
		40	3010.3	12.6
		80	3008.6	12.8
N_2+CH_4 (1:1)	–	0	3011.7	10.1
CH_3OH	He^+ 3 keV	52	3009.5	11.0

amount of each species in the mixture. In fact the assumption that the species deposit in the same ratio as they are prepared in the mixing chamber might in some case be incorrect. Thus in the following we will assume that the integrated absorbance of CH_4 bands does not change in mixtures.

Fig. 3 shows the band profile in different ice mixtures containing CH_4 for different irradiation doses. Fig. 4 shows the band profile as produced after ion irradiation of ice mixtures containing CH_3OH and H_2O at different ratios. Table 2 lists peak positions and widths of the band in all the samples ex-

Table 5. Position (cm^{-1}) and FWHM (cm^{-1}) of the 1302 cm^{-1} band of CH_4 in various irradiated and unirradiated ice mixtures upon warm-up.

Initial mixture	T (K)	Peak (cm^{-1})	FWHM (cm^{-1})
pure CH_4 as deposited	12.5	1301.5	6.7
	16	1299.8	6.0
	20	1299.7	6.4
	25	1299.6	7.0
	30	1299.4	8.0
	35	1299.4	9.0
pure CH_4 + 170 eV/16 a.m.u.	12.5	1300.3	9.7
	20	1299.8	9.4
	25	1299.7	9.3
	30	1299.6	9.3
	35	1299.4	9.5
H_2O+CH_4 (1:1) as deposited	10	1300.6	12.0
	17	1300.4	11.3
	27	1300.3	10.4
	47	1302.4	10.5
	67	1302.7	10.1
	107	1303.1	10.6
H_2O+CH_3OH (2:1) + 40 eV/16 a.m.u.	10	1303.4	12.8
	47	1303.8	10.9
H_2O+CH_3OH (1:1) + 44 eV/16 a.m.u.	10	1303.3	10.9
	151	1303.6	10.0
CH_3OH + 40 eV/16 a.m.u.	10	1303.2	10.3
	47	1302.9	10.0
	97	1303.0	10.9
	147	1303.1	13.8

amined, at various irradiation doses, before warming up. The peak position of the C-H deformation mode of CH_4 was found to range between 1299.3 to 1304.0 cm^{-1} in the examined ice mixtures. The gas phase position of the origin of the band lies at 1305.5 cm^{-1}, so that the band appears always more or less redshifted, indicating an attractive interaction with the solid matrix. The highest redshift was observed for CH_4 codeposited with NH_3, even higher than that observed for pure CH_4 at low temperatures, while the lowest was observed for CH_4 produced irradiating CH_3OH or mixtures of CH_3OH and water with energetic ions. The full width at half maximum, at low temperatures, ranges from 6.7 cm^{-1} in pure CH_4 as deposited to 13.8 cm^{-1} in H_2O+NH_3+CH_4 as deposited. It can be seen that, exception made for pure CH_4, the general trend is that this band shifts, if any, to slightly higher wavenumbers and gets narrower for higher irradiation doses. It can also be seen that, in all samples examined, if CH_4 is produced by ion irradiation of ice mixtures containing CH_3OH, the band tends to peak at higher wavenumbers. Where comparable, our results agree closely with those published by Boogert et al. (1997).

Table 6. Position (cm^{-1}) and FWHM (cm^{-1}) of the 3010 cm^{-1} band of CH_4 in various irradiated and unirradiated ice mixtures upon warm-up.

Initial mixture	T (K)	Peak (cm^{-1})	FWHM (cm^{-1})
pure CH_4 as deposited	12.5	3009.2	5.2
	16	3010.9	12.3
	20	3011.0	13.2
	25	3011.0	15.4
	30	3010.9	18.2
	35	3010.9	20.0
pure CH_4 + 170 eV/16 a.m.u.	12.5	3008.9	10.5
	20	3008.8	11.6
	25	3008.4	12.0
	30	3008.5	13.1
	35	3008.0	14.0
H_2O+CH_4 (1:1) as deposited	10	3010.0	11.9
	17	3010.0	11.8
	27	3010.2	12.3
	47	3008.7	18.2

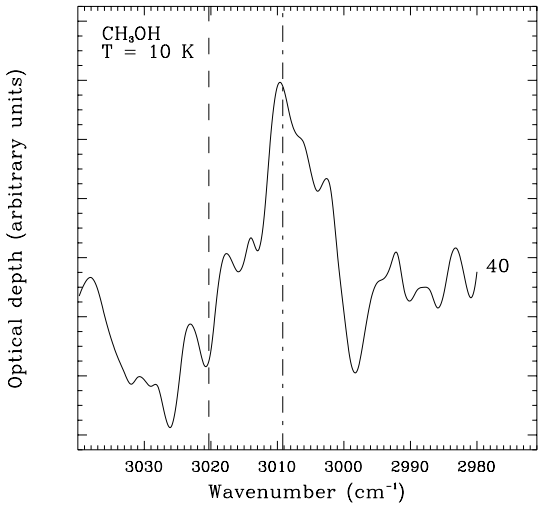

Fig. 6. The spectrum of the band at 3010 cm^{-1} of CH_4 produced by ion irradiation of CH_3OH. The position of the origin of the band in gaseous CH_4 (3020.3 cm^{-1}) is indicated by the dashed line, the position of the peak in pure CH_4 ice as deposited (3009.2 cm^{-1}) is indicated by the dash-dotted line.

3.2. The 3010 cm^{-1} C-H stretching mode

Fig. 1b shows the profile of the ν_3 mode for pure CH_4 at T = 12.5 K, in optical depth scale and normalized to unit integrated area, at the end of the deposition. It shows a considerable structure, and can be fitted with a superposition of five pseudo-voigt functions with the parameters given in Table 3. As before, the choice of such functions was simply one of convenience. The fitted profiles are shown dotted in Fig. 1b. Clearly, the superposition of the second and third function reproduces the profile of the main peak, while the others seem to represent

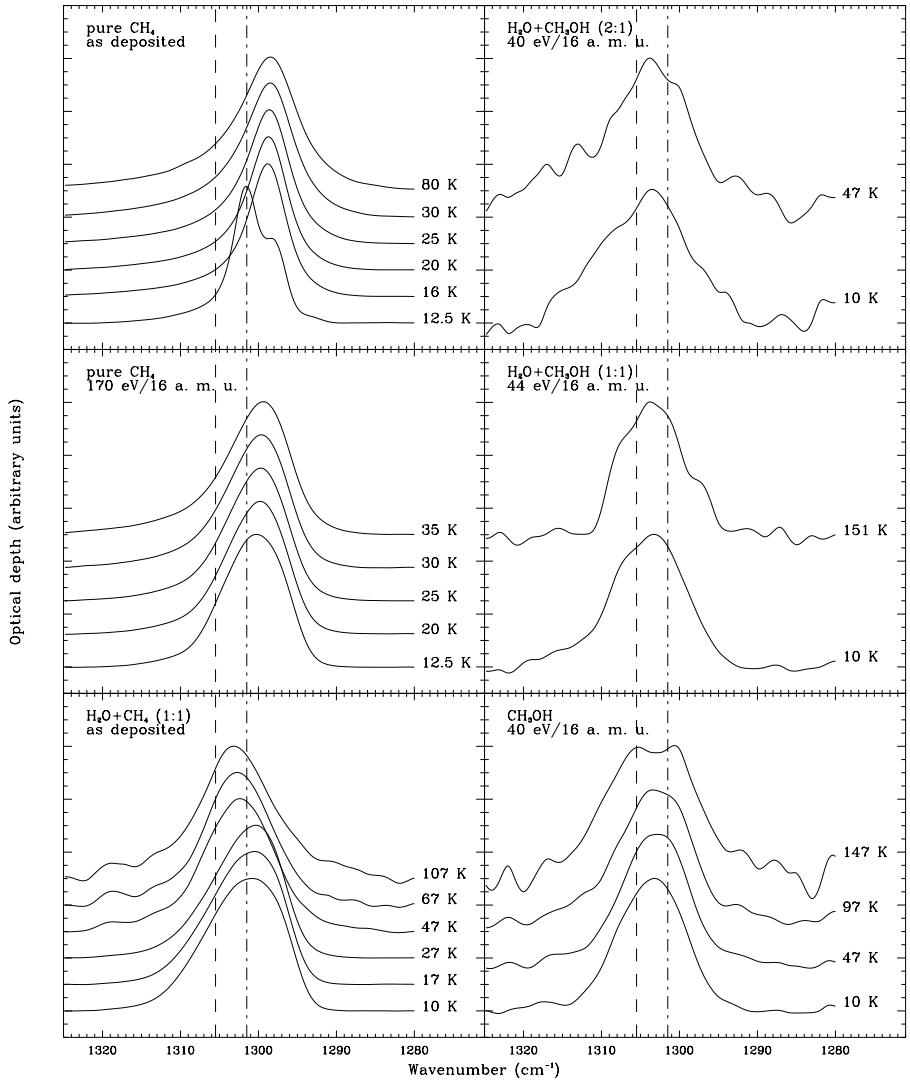

Fig. 7. Variations of the shape and position of the CH_4 band at 1302 cm^{-1} in irradiated and unirradiated ice mixtures upon warm-up. The initial mixture is indicated in top left corner of each box, along with the dose, in units of eV/16 a. m. u.. The temperature is indicated beside each plotted band. The position of the origin of the band in gaseous CH_4 (1305.5 cm^{-1}) is indicated by the dashed line, the position of the peak in pure CH_4 ice as deposited (1301.5 cm^{-1}) is indicated by the dash-dotted line.

real fine structure. The first one is very weak and might be simply noise, even though it is consistently present in all spectra taken at different thicknesses of the sample, as the parameters were derived from a *combined* fit of all these spectra. Moreover, such structures are expected to appear in CH_4 due to the breaking of symmetry of the higher vibrational level involved in the transition by the crystal electric field and to the presence of different nonequivalent sites (see, for example, Bohn et al., 1994). Again, to measure the integrated absorbance we used all the spectra taken at different thicknesses of the sample, during deposition. The slope of the straight line through the origin fitted to the data yields a value of $9.5 \cdot 10^{-18}$ cm $\cdot$ mol^{-1}. The data and the fitted line are shown in Fig. 2b. Using the data from the paper of Hudgins et al. (1993), assuming for pure CH_4 ice a density of 0.52 g cm^{-3} (Landolt-Börnstein 1971), as done by Boogert et al. (1997) for the band at 1302 cm^{-1}, one derives a value of $11.0 \cdot 10^{-18}$ cm $\cdot$ mol^{-1}, which is again somewhat larger than our measurement.

Fig. 5 shows the band profile in different ice mixtures containing CH_4 for different irradiation doses. Fig. 6 shows the band profile as produced after ion irradiation of CH_3OH. It is evident that the signal to noise ratio in this band is generally much worse, especially when water is present in the ice mixture, since this band lies on top of a very strong and broad water band that has to be subtracted first. Table 4 lists peak positions and widths of the band in all samples examined, at various irradiation doses, before warming up. The peak position of the C-H stretching mode of CH_4 was found to range between 3007.7 to 3011.7 cm^{-1} in the examined ice mixtures. The gas phase position of the origin of the band lies at 3020.3 cm^{-1}, so that the band appears again more or less redshifted. The highest redshift was observed for CH_4 codeposited with NH_3, just as for the C-H deformation band, while the lowest was observed for CH_4 codeposited with N_2. The full width at half maximum, at low temperatures, ranges from 5.2 cm^{-1} in pure CH_4 as deposited to 14.7 cm^{-1} in H_2O+NH_3+CH_4 as deposited, again just as for the other fundamental band.

3.3. Warm-up effects

Figs. 7 and 8 show the evolution of the band profiles of the C-H deformation and the C-H stretching upon warming up the irradiated and unirradiated samples. Tables 5 and 6 list measured peak positions and FWHMs. Generally, the band at 1302 cm^{-1} changes much less than that at 3010 cm^{-1} with temperature. The band at 1302 cm^{-1} always gets slightly narrower at first to get wider again at higher temperatures only in some of the samples. The peak position of this band changes very little, except for pure CH_4 and H_2O+CH_4 (1:1) as deposited, for which phase changes suggested by abrupt changes in the profile of the bands can be clearly seen respectively between 12.5 and 16 K (see CH_4 in Figs. 7 and 8) and between 27 K and 47 K (see H_2O+CH_4 (1:1) in Fig. 7). The band at 3010 cm^{-1} is, on the other hand, extremely sensitive to the temperature in all the samples in which it was detected. Its width always increases greatly upon warm-up, particularly in pure CH_4, for which it changes from 5.2 to about 20 cm^{-1}. Again, variations in the peak position are much smaller. The strong variations in width may result from a competition between annealing, that tends to reduce the number of different nonequivalent sites that a CH_4 molecule can occupy, and another mechanism, that might be hindered rotation (Jones et al., 1986; Nelander, 1985), that tends to increase the width of the bands. However, it is clear that the band at 3010 cm^{-1} is much more sensitive to temperature changes than that at 1302 cm^{-1}. Since both bands arise from transitions from the fundamental level to a vibrational level of the same species, if their widths were due to unresolved hindered (almost free) rotational structure, one would expect them to be very similar at all temperatures, and especially to have similar widths in energy scale. Since this is not the case, not even for pure CH_4, either hindered rotation is not the sole cause of broadening, or the molecule rotation must be rather differently hindered in the two different excited vibrational states. Our measuments of the peak positions of the bands at 1302 cm^{-1} and 3010 cm^{-1} of pure CH_4 as deposited at various temperatures, upon comparison with those by Hudgins et al. (1993) at 10, 20 and 30 K, are very close but systematically shifted to slightly lower wavenumbers with respect to them, by about 0.5 cm^{-1}.

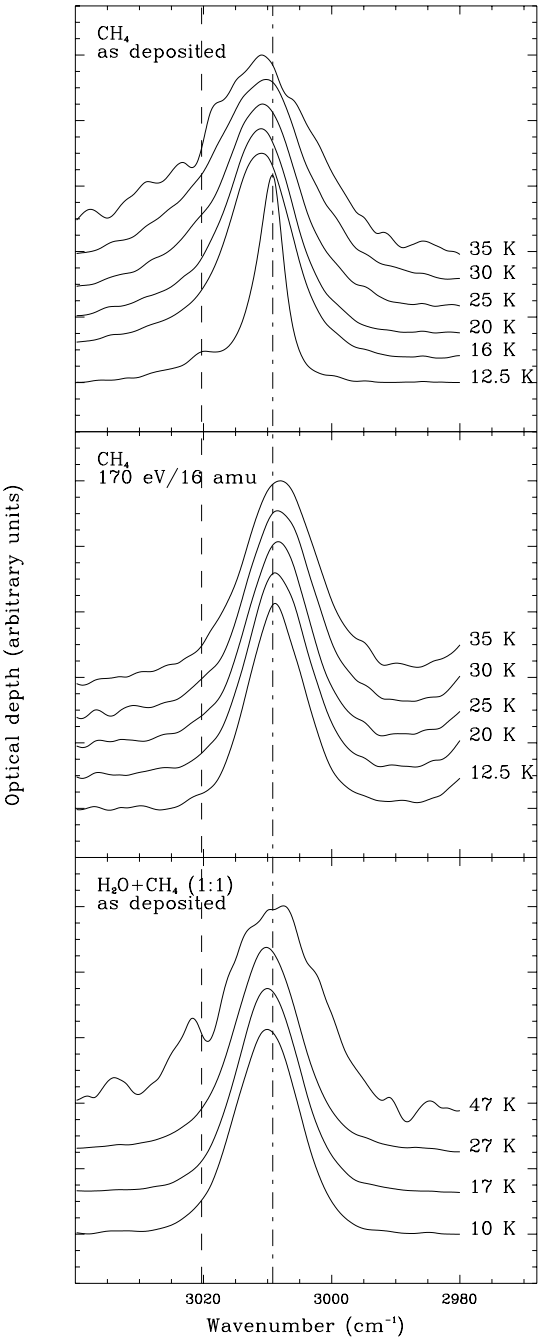

Fig. 8. Variations of the shape and position of the CH_4 band at 3010 cm^{-1} in various ice mixtures upon warm-up. The initial mixture is indicated in top left corner of each box, along with the dose, in units of eV/16 a. m. u.. The temperature, in K, is indicated beside each plotted band. The position of the origin of the band in gaseous CH_4 (3020.3 cm^{-1}) is indicated by the dashed line, the position of the peak in pure CH_4 ice as deposited (3009.2 cm^{-1}) is indicated by the dash-dotted line.

4. Final remarks

The flux of low energy cosmic rays in the interstellar medium is not well known. A proton flux $J(E = 1\text{MeV}) \approx 3\ \text{cm}^{-2}\,\text{s}^{-1}$ has been estimated by Jenniskens et al. (1993). The specific energy loss of 1 MeV protons in a typical grain containing heavy atoms (C, N, O, Si) is $S \sim 5 \cdot 10^{-15}$ eV cm^2/atom. Greenberg (1982) estimated lifetimes of dense clouds to be of $3 \cdot 10^7 - 5 \cdot 10^8$ years. Assuming a gas density $n_0 \sim 10^4\ \text{cm}^{-3}$, it takes $10^9/n_0 \simeq 10^5$ years for icy mantles to condense on grains (Tielens & Allamandola 1987). These frozen mantles suffer ion irradiation for $10^5 - 10^8$ years ($3 \cdot 10^{12} - 3 \cdot 10^{15}$ sec). The former estimate refers to the case of mantles which evaporate immediately after formation while the latter refers to the limiting case of mantles which survive, at least partly, for all the cloud lifetime (Palumbo & Strazzulla 1993). Therefore, after a time t of $3 \cdot 10^{12} - 3 \cdot 10^{15}$ sec the energy deposited on an icy grain mantle (dose) is given by $S \cdot J \cdot t$ and values 0.05−50 eV/atom(C,N,O,Si).

Laboratory experiments and theoretical models had predicted the presence of CH_4 in icy grain mantles. This had been

confirmed by ground and airplane based observations first (Lacy et al., 1991; Boogert et al., 1997) and ISO observations recently (Boogert et al., 1996). They revealed the C-H deformation band of frozen CH_4 with a peak position of 7.67 μm and a FWHM of 0.062 μm, corresponding respectively to 1303.8 and 10.5 cm^{-1}. This fits nicely with the limits we found in our experiments, and especially with the position and FWHM we found for polar mixtures containing CH_3OH where CH_4 is produced by ion irradiation. However, as was pointed out by Boogert et al. (1997), there are various ice mixtures containing CH_4 that are compatible with the observed spectra, so that no unique identification is possible at present. A more sensitive test would be to observe the interstellar C-H stretching band of CH_4, but this has not been achieved thus far. If this is finally done, the direct comparison of the two bands with our (and other) laboratory spectra will give precious information about the environment and irradiation history of the grain mantles containing CH_4. This will be possible when the data of the ISO observations will be publicly available.

References

Baratta G.A., Spinella F., Leto G., Strazzulla G., Foti G., 1991, A&A 252, 421

Bohn R.B., Sandford S.A., Allamandola L.J., Cruikshank D.P., 1994, Icarus 111, 151

Boogert A.C.A., Schutte W.A., Tielens A.G.G.M., et al., 1996, A&A 315, L377

Boogert A.C.A., Helmich F.P., Schutte W.A., Tielens A.G.G.M., Wooden D.H., 1997, A&A 317, 929

Greenberg M.J., 1982, What are comets made of? A model based on interstellar dust. In: Wilkening L.L. (ed.) Comets. The Univ. of Arizona Press, Tucson, 131

Herbst E., Leung C.M.,1986, MNRAS 222, 689

Herzberg G., 1991, Molecular spectra and molecular structure, vol. II, Infrared and Raman spectra of polyatomic molecules, Krieger Publishing Company

Hudgins D.M., Sandford S.A., Allamandola L.J., Tielens A.G.G.M., 1993, ApJS 86, 713

Jenniskens P., Baratta G.A., Kouchi A., et al., 1993, A&A 273, 583

Johnson R.E., Energetic charged-particle interactions with atmospheres and surfaces, 1990, Lanzerotti L.J. (ed.), Springer Verlag Press

Jones L.H., Ekberg S.A., Swanson B.I., 1986, J. Chem. Phys. 85, 3203

Lacy J.H., Carr J.S., Evans II Neal J., et al., 1991, ApJ 376, 576

Landolt-Börnstein, 1971, Zahlenwerte und Funktionen. Springer-Verlag, Berlin, II. Band, 1. Teil, 471

Millar T.J., Nejad L.A.M., 1985, MNRAS 217, 507

Moore M.H., Hudson R.L., 1992, ApJ 401, 353

Moore M.H., Donn B., Khanna R., A'Hearn M.F., 1983, Icarus 54, 388

Nelander B., 1985, J. Chem. Phys. 82, 5340

Palumbo M.E., Strazzulla G., 1993, A&A 269, 568

Spinella F., Strazzulla G., Baratta G.A., 1991, Rev. Sci. Instrum. 62, 1743

Tielens A.G.G.M., Allamandola L.J., 1987, Evolution of Interstellar Dust. In: Morfill G.E., Schoeler M. (eds.) Physical Processes in Interstellar Clouds. Reidel Dordrecht, 333

Tielens A.G.G.M., Hagen W., 1982, A&A 114, 245

Strazzulla, G., Baratta, G.A., 1992, A&A 266, 434

Strazzulla G., Brucato J.R., Palumbo M.E., Satorre M.A., 1997, A&A 321, 618